Russian Journal of Earth Sciences

Comparative Analysis of Eddies in Open Ocean and Marginal Ice Zone Using SWOT and Sentinel-1 Data

N. V. Sandalyuk[1,2,*] and E. M. Khachatrian[3,4]

[1] The Moscow Institute of Physics and Technology, Dolgoprudny, Moscow Region, Russia
[2] Saint Petersburg State University, Saint Petersburg, Russia
[3] UiT The Arctic University of Norway, Tromsø, Norway
[4]GEOFEM, Nicosia, Cyprus
* **Correspondence to:** Nikita Sandalyuk, nikitasandaliuk@gmail.com

Abstract: The new Surface Water and Ocean Topography (SWOT) mission, featuring unprecedented resolution and precision, represents a new era in satellite altimetry and exploration of ocean eddy dynamics. This paper provides a specific test case for the inter-comparison of eddy fields in the open ocean and the Marginal Ice Zone in the Fram Strait, utilizing Synthetic Aperture Radar (SAR) data and a complementary Level 3 product from the SWOT altimetry mission. We identified and matched 7 occurrences of open ocean eddies from both data sources. A crucial and anticipated finding is that the SSHA fields demonstrate clear capability in resolving small (up to 10 km) submesoscale eddies. The comparison of the SAR and backscattering coefficient from the SWOT unsmoothed fields for the Marginal Ice Zone region revealed a generally good agreement between both data types and can be used by the researchers as complementary data sources.

Keywords: SWOT, Sentinel-1, SAR, submesoscale-mesoscale eddies, Fram Strait

Citation: Sandalyuk N. V. and Khachatrian E. M. (2026), Comparative Analysis of Eddies in Open Ocean and Marginal Ice Zone Using SWOT and Sentinel-1 Data, *Russian Journal of Earth Sciences*, 26, ES1003, EDN: ASSZDJ, https://doi.org/10.2205/2026es001081

1. Introduction

For the last three decades, satellite altimetry has been the main source of information about global ocean surface dynamics. The merging of measurements from multiple altimetry missions has led to the construction of the reprocessed gridded datasets (L4) [*Pujol et al.*, 2016], which have significantly increased our understanding of large-scale ocean dynamics, particularly the physics and kinematics of mesoscale eddies [*Belonenko et al.*, 2023; *Chelton et al.*, 2011; *Faghmous et al.*, 2015; *Gnevyshev et al.*, 2021; *Malysheva et al.*, 2020; *Sandalyuk et al.*, 2020a; *Sandalyuk and Belonenko*, 2018; *Sandalyuk et al.*, 2020b; *Travkin and Belonenko*, 2019]. However, the spatial limitations of the L4 products ($0.25° \times 0.25°$) leave structures with spatial scales under 30 km essentially unobserved. These limitations are especially important for the study of eddies in the polar regions since the Rossby radius of deformation is significantly smaller in the high latitudes (~10–15 km), and only a fraction of eddies can be detected from the altimetry fields in this area. It should also be mentioned that the Rossby radius of deformation is much smaller on the Arctic shelf due to shallow depth. Therefore, information about eddies with spatial scales under 30 km is heavily overlooked. The current spatial resolution of the altimetry L4 products makes it impossible to utilize the altimetry data in the studies of the submesoscale eddy structures.

A new satellite mission, SWOT (Surface Water and Ocean Topography), was launched in December 2022. It carries the two KaRIns (*Ka*-band Radar Interferometer) [*Tréboutte et al.*, 2023]. KaRIn represents a synthetic aperture radar interferometer with two swaths of 50 km each [*Morrow et al.*, 2019]. The KaRIn is a bistatic SAR system operating at a frequency of 35.75 GHz (wavelength of 8.4 mm). The system consists of two antennas separated by a 10 m mast, which measure the Earth's surface in a near-nadir look angle

Research Article

Received: April 23, 2025
Accepted: November 5, 2025
Published: February 20, 2026

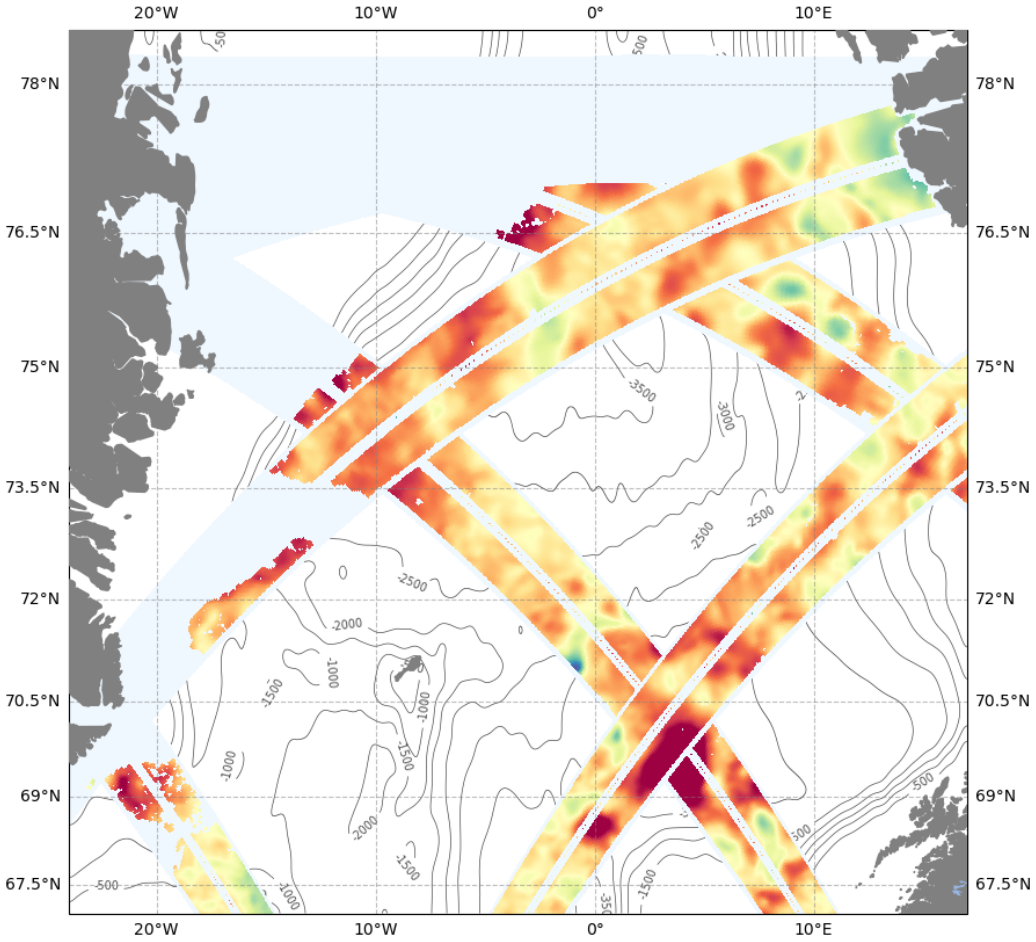

Figure 1. The map of the study region with overlaid SWOT passes for the 1-day revisit CalVal orbit on 09.06.2023. The rapid color change in the western area (from red to light blue) indicates the beginning of the MIZ.

ranging between ~ 1° and ~ 4°. One antenna emits radar signals, and both antennas receive the radar backscattered signals. The whole load-up provides a 120 km wide swath of coverage (including the 20 km nadir gap), resulting in the SSHA (Sea Surface Height Anomaly) field with the resolution of 2 km [*Dibarboure et al.*, 2022; *Tréboutte et al.*, 2023]. SWOT is also equipped with a conventional nadir altimeter that provides along-track measurements within the 20 km coverage gap. The new mission has unprecedented resolution and precision, thus representing a new era in satellite altimetry and exploration of ocean dynamics. The initial SWOT data reveal that the spectral noise level is an order of magnitude lower than the original science requirement at small scales, enabling the observation of ocean circulation processes at scales as fine as ~ 5 km [*Fu et al.*, 2024]. The nominal life of the mission is 42 months, with the first 3 months for engineering checkout, followed by 3 months for calibration and validation, then a minimum of 36 months for global mapping [*Fu et al.*, 2024].

One of the main objectives of the SWOT mission is to study submesoscale processes in the ocean. We expect that the new data from the SWOT mission will significantly improve our understanding of mesoscale fields and especially submesoscale processes, such as eddy dynamics. This is crucial information not only for estimating the kinetic energy of ocean circulation but also for the ocean uptake of heat and carbon, which plays a key role in climate change [*Morrow et al.*, 2019].

Apart from radar altimetry, other sensors can also be used to retrieve information about mesoscale and submesoscale eddies in the polar regions. At the present moment, the most advanced and versatile source of information on eddy dynamics in polar regions is synthetic aperture radar (SAR). SAR sensors operate at various modes that have different

characteristics, namely frequency bands, polarization channels, spatial resolutions, and coverage. It mainly responds to the surface dielectric properties, geometry, and roughness. Depending on the frequency or wavelength, which determines penetration depth, it can refer to either the volume or the surface structure of the target. The SAR measurements are solar and cloud-independent and provide high spatial resolution up to several meters. The data from SAR satellite sensors are commonly used in studies that focus on the open ocean arctic eddies [*Atadzhanova et al.*, 2017; *Bashmachnikov et al.*, 2020; *Cassianides et al.*, 2021] as well as the eddies in the marginal ice zone (MIZ) [*Khachatrian et al.*, 2023; *Kozlov et al.*, 2019, 2020]. Moreover, the SAR data are commonly used to study submesoscale eddies in various regions of the World Ocean [*Karimova and Gade*, 2015; *Xia et al.*, 2022]. We anticipate that SAR measurements and data from the new SWOT mission will complement each other in capturing mesoscale and submesoscale eddy dynamics, particularly in polar regions. Examining the relationship between these two datasets could provide insights into the extent to which the SSHA fields from SWOT can represent small eddies visible in SAR scenes. Additionally, there is potential for SWOT's unsmoothed backscatter signal to aid in detecting eddies in the MIZ, which warrants further consideration.

The Level 3 (L3) products are produced and distributed publicly to facilitate the validation of SWOT/KaRIn data. The altimetry and SWOT community encourages oceanographers for the early evaluation of SWOT products early in their areas of expertise. Since we are highly interested in the evaluation and further usage of the SWOT data in our research, we conducted this study as a response to the community request for early validation of the SWOT data, as well as to improve our understanding of the further implementation of the SWOT data in our studies and to develop a necessary methodology.

This study investigates oceanic eddies in the Fram Strait, a region known for its dynamic oceanographic conditions. The Fram Strait is characterized by frequent eddy formation, both in the MIZ and the open ocean, playing a significant role in heat, salt, and nutrient redistribution, which affects oceanographic, sea ice, and biological properties [*Bashmachnikov et al.*, 2020; *Kozlov and Atadzhanova*, 2021; *Wekerle et al.*, 2020]. The main drivers of eddy generation in the Fram Strait region are baroclinic and barotropic instability of the West Spitsbergen and East Greenland Currents, combined with the currents' interaction with complex bathymetry [*Bashmachnikov et al.*, 2020; *Kozlov and Atadzhanova*, 2021; *Wekerle et al.*, 2020]. The average ratio between numbers of cyclonic and anticyclonic eddies is 3:1, which is typical for the mesoscale dynamics in this region [*Kozlov and Atadzhanova*, 2021], and in line with observations in eddy-active regions of the Global Ocean [*Chelton et al.*, 2011]. The estimation of the average Rossby radius of deformation in the Fram Strait is 4–6 km in summer and 3–4 km in winter periods [*Appen et al.*, 2016]. However, due to the stronger stratification during the ice-free season, it can go up to 10–15 km [*Nurser and Bacon*, 2013]. Previous research has reported that mean eddy diameters in the region range from approximately 6 km in shallow waters to 12 km in deeper regions [*Kozlov and Atadzhanova*, 2021], though these values exhibit substantial variability depending on the dataset and methodology used. Typical eddies in the Fram Strait are often too small to be detected by conventional altimetry products, especially those with diameters under 20 km. As a result, standard satellite observations struggle to resolve them, underscoring the need for higher-resolution data to capture the full spectrum of eddy sizes in the region. Moreover, the size and behavior of eddies are influenced by various factors, including oceanic conditions and seasonal variability, which complicate their characterization. Understanding these dynamics is essential for improving oceanographic models and advancing our knowledge of Arctic climate processes.

The primary objective of this case study is to compare eddy signatures detected in Sentinel-1 SAR imagery with corresponding eddy structures derived from SWOT L3 data, across both open-ocean and MIZ environments. Furthermore, this work aims to assess the degree of agreement between these complementary datasets to identify their respective strengths and limitations. Accordingly, we provide a detailed visual analysis of eddies identified from each source, accompanied by a characterization of their structural and geometric distinctions.

The rest of this paper is organized as follows. Section 2 shows the datasets and methods used in this study. Section 3 presents an analysis and experimental results. Finally, the discussion and conclusions are presented in Section 4.

2. Data and Methods

2.1. SWOT

The present state of the SWOT mission is still CalVal (Calibration and Validation phase) with the current state of the L2/L3 product being "beta prevalidated" [*AVISO*, 2023; *SWOT*, 2023]. We are aware that the data might exhibit some artifacts, limitations, and noise. The further releases will be followed by many upgrades in terms of corrections, noise mitigation, etc [*SWOT*, 2023]. Both L2/L3 products contain data from two periods. The first period covers the time span of March–July 2023 and contains measurements from the CalVal orbit with a revisit time of one day and sparse coverage (Figure 1). The second period includes a time span of September–November 2023 and contains measurements from the "science" orbit, which has a 21-day revisit time with global coverage for latitudes below 78° [6]. Despite the sparse coverage of the CalVal orbit, the one-day revisit time significantly simplifies the constant eddy monitoring for the chosen region. Hence, almost all detected eddies were obtained for the CalVal orbit data. The L2/L3 SWOT data are publicly available through the AVISO website (https://www.aviso.altimetry.fr/). The L3 dataset was acquired for the whole available measurement period (March–November 2023). The L2 unsmoothed data were acquired only for certain dates (02–03.2023, 07.07.2023, 03.11.2023).

2.1.1. Level 2

The L2 product contains data from the low-rate data stream of the SWOT KaRIn instrument and provides sea surface height (SSH) and σ_0 without additional smoothing relative to the native KaRIn downlink resolution on a 250 m native (center-beam) grid [*SWOT*, 2023]. This is the expert-level go-to product for technical and expert algorithm analyses, as well as instrument and algorithm research. In our study, we use σ_0 or the backscattering coefficient to check the possibility of using this type of data for detecting eddies in the MIZ. Applying $\log^2(\sigma_0)$ reveals finer small-scale details.

2.1.2. Level 3

The L3 data have been derived from updated Level-3 algorithms and reprocessed beta-prevalidated Level-2 KaRIn Low Rate ocean products. The product has been put through the process of multimission calibration [*Faugére et al.*, 2022], noise mitigation (AI-based) [*Gómez-Navarro et al.*, 2020; *Tréboutte et al.*, 2023], and various geophysical corrections have been implemented (e.g., tides). Both measurements from KaRIn and nadir instruments are blended into a single 2-km product. We use an L3 basic (lightweight) product that contains only SSHA and mean dynamic topography [*AVISO*, 2023]. This is a simple and easy-to-use out-of-the-box product that does not require any expert knowledge of altimetry. The example of the SWOT passes of the L3 product is presented in Figure 1. It should also be noted that we have not implemented any kind of additional smoothing or interpolation for the visualization of the SSHA fields.

2.2. ADT

ADT(Absolute Dynamic Topography) is the instantaneous height above the Geoid. The ADT variable is obtained by adding an MDT (Mean Dynamic Topography) to the Sea Level Anomaly (SLA) field. The SLA is calculated by Optimal Interpolation, merging the L3 along-track measurement from various available altimeter missions [*Copernicus*, 2024]. This L4 product is processed by the Data Unification and Altimeter Combination System (DUACS). The dataset is publicly available on the Copernicus Marine Environment Monitoring Service website (https://marine.copernicus.eu/).

2.3. SAR

The Sentinel-1 data are publicly available through Copernicus Open Access Hub (https://dataspace.copernicus.eu/), the European Union's Earth observation programme [*ESA*, 2024]. Sentinel-1 operates at the *C*-band with a central frequency of 5.404 GHz. It includes two polar-orbit Sentinel-1A and Sentinel-1B missions that provide multiple sensing modes in single or dual polarization. For this study, we acquired the Sentinel-1 Level-1 Ground Range Detected images in extra-wide swath mode in dual-polarization (HH and HV) at 40 m spatial resolution. In addition, we performed several preprocessing steps, including correcting for thermal and speckle noise, and calibration to σ_0 in dB using the ESA Sentinel-1 Toolbox.

2.4. Eddy Identification

The detection of oceanic eddies from both SAR and SWOT data is conducted through a systematic visual examination of satellite images. This approach leverages the high-resolution capabilities of SAR imagery and the precise altimetric measurements from SWOT to identify and analyze mesoscale and submesoscale eddies in the study area.

The following approach includes several steps:

Step 1. *Assessing SWOT Spatial Coverage.* The first step in the detection process involves verifying the spatial coverage of SWOT passes over the study region.

Step 2. *Selecting and Aligning SAR Data.* Once the SWOT coverage has been mapped, we proceed to examine SAR imagery that coincides both spatially and temporally with the SWOT overpasses.

Step 3. *Identifying Eddy Signatures in SAR Imagery.* Eddy identification within SAR images is based on visually interpreting their characteristic spiral patterns (see Figure 2a, c, e), Figure 4a, c, e, h) and as depressions or elevations in the SSHA fields (Figure 2b, d, f). The eddy centers are defined as the geometric centers of eddies, which are approximated as ellipsoids in the SAR images and as local min/max values in the SSHA fields.

Step 4. *Cross-Referencing with SWOT Data.* Once eddies have been visually identified in SAR images, their locations are cross-referenced with SSHA fields from SWOT.

Step 5. *Classification and Documentation.* The final step involves categorizing the detected eddies based on their polarity (cyclonic or anticyclonic) and determination of eddy scale. The eddy scale is defined as the average of the major and minor axis lengths of the ellipse that approximates the eddy's shape.

The visual method for identifying eddies from SAR images has been employed in numerous studies focusing on eddy research from SAR data [*Atadzhanova et al.*, 2017; *Kozlov et al.*, 2019; *Kozlov and Atadzhanova*, 2021; *Kozlov et al.*, 2020; *Zimin et al.*, 2021]. It should be noted that the visual methods are generally prone the subjectivity and interpretations may vary between analysts. However, the steps and criteria outlined for visual eddy detection are unambiguous and leave little room for misinterpretation, provided that SAR data are supported by additional source of information on eddy location.

3. Experimental Results and Discussion

This section presents a comparison of eddy signatures detected from both Sentinel-1 SAR scenes and corresponding SSHA fields from SWOT passes in the open ocean and MIZ areas. Table 1 specifically summarizes the most important characteristics of eddies used in this study.

3.1. Open Ocean Eddies

Based on a visual examination, we detected 7 instances of eddies that were identified on both SAR images and SSHA fields in the open ocean. Overall, there are three cases on three separate dates. The first case represents two cyclonic eddies and one anticyclonic

Table 1. Characteristics of eddy signatures detected from the Sentinel-1 and SWOT missions in the open ocean and MIZ scenarios. The scale parameter represents the approximate size of eddies (average of semi-major and semi-minor axes of an eddy elliptical contour)

Open Ocean Eddies			
Date	Number of Eddies	Scale (km)	Polarity
28.04.2023	3	30	cyclonic
		25	anticyclonic
		15	cyclonic
22.06.2023	2	50	anticyclonic
		30	cyclonic
09.07.2023	2	20	cyclonic
		10	anticyclonic
Eddies in Marginal Ice Zone			
02.07.2023	2	30	cyclonic
		15	cyclonic
03.07.2023	2	25	cyclonic
		15	cyclonic
07.07.2023	1	10	cyclonic
03.11.2023	1	60	anticyclonic

(Figure 2a–b) on date 28.04.2023, which are clearly detectable on both images. The approximate spatial scales of the eddies are 30 km (cyan dot), 15 km (green dot), and 25 km (pink dot). It is quite hard to unambiguously define eddy polarity from the SAR image, which presents a traditional problem for a certain fraction of eddies detected from SAR, especially for the open ocean eddies [*Zimin et al.*, 2021]. However, the eddy vorticity sign becomes clear from SSHA data. There is also an observed bias between eddy centers from SAR and SWOT data. The average displacement between eddy centers identified in SAR images and SSHA fields is 3 km, while in certain cases it can be up to 5 km. The bias can be explained by the difference in the time the satellites pass and the related time shift of the eddy location, as well as the fact that the maximum eddy amplitude value is not necessarily located in the geometrical eddy center [*Chelton et al.*, 2011].

The second case represents two eddies (cyclonic and anticyclonic) (Figure 2c–d) on a date of 22.06.2023. The approximate spatial scales of eddies are 50 km (cyan dot) and 30 km (pink dot). The SAR image reveals a highly turbulent field, which significantly complicates the eddy detection. However, the comparative analysis of the synchronous SSHA field from the SWOT helps us to identify two distinct eddies.

The third case represents two eddies (cyclonic and anticyclonic) (Figure 2e–f) on a date 09.07.2023. The approximate spatial scales of the two identified eddies are 20 km (pink dot) and 10 km (cyan dot). This particular case is the most problematic for visual interpretation, primarily due to the observed shift between eddy centers from SAR and SWOT data. However, after a close examination of both data sources and a comparison of the vorticity signs, we managed to match the eddies detected from the SAR scene with the eddy signatures from SWOT data [*Chelton et al.*, 2011].

Additionally, we compared eddies detected from SAR images and complementary SSHA fields with the ADT fields on the same dates and locations (Figure 3). The ADT data were acquired from the L4 merged altimetry product, which is traditionally used for eddy detection and tracking [*Chelton et al.*, 2011; *Faghmous et al.*, 2015]. As we expected, significantly large eddies are detectable from ADT, but starting from sizes of approximately 25 km and below, the eddies become undetectable from L4 fields. The observed difference demonstrates how the interpolation in the absence of measurements for a specific area and date can substantially distort the true state of physical reality.

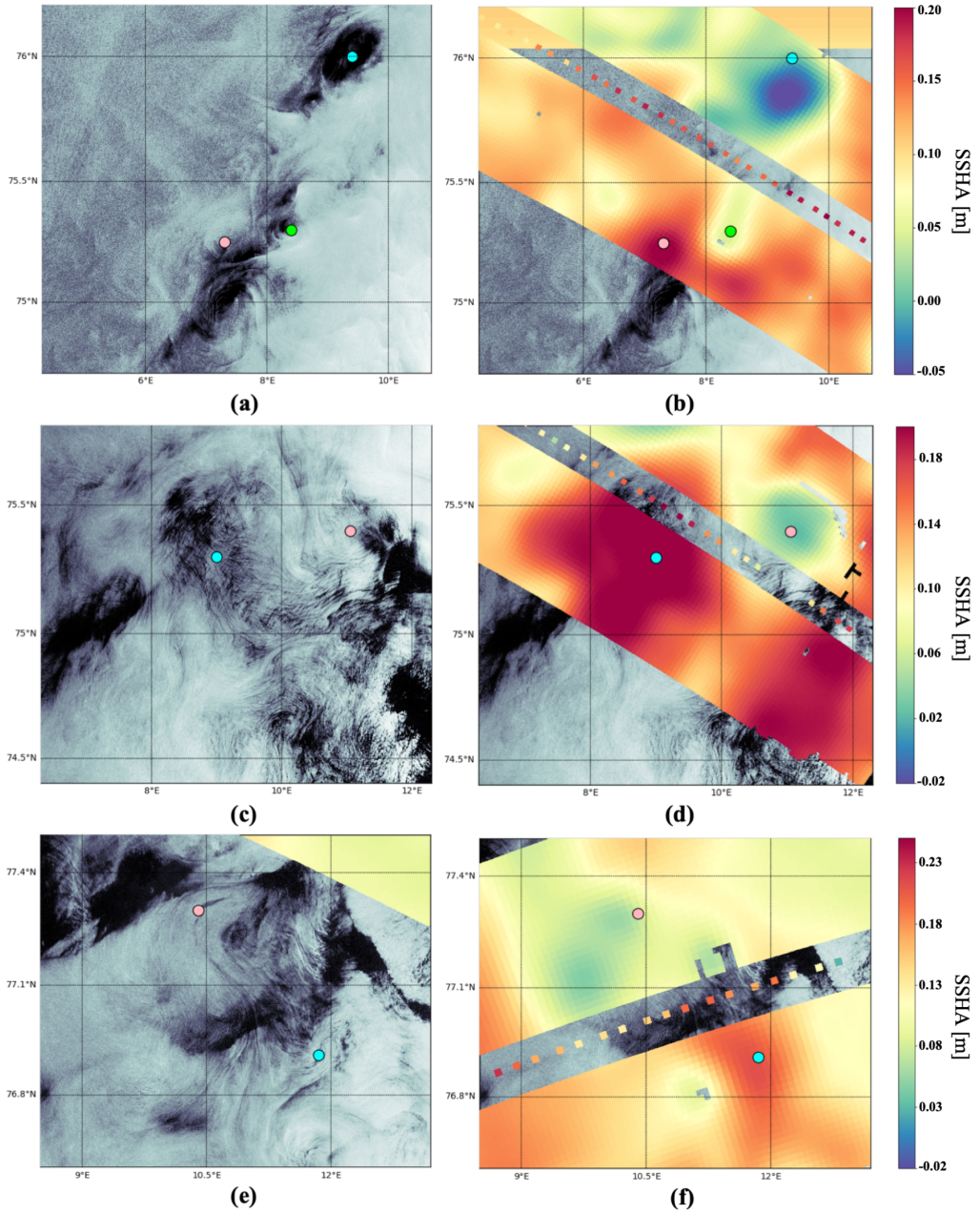

Figure 2. SAR image (left column) and combined SAR and overlaid SSHA from SWOT passes (right column) on the same dates: 28.04 (a–b), 22.06 (c–d), 09.07 (e–f) of 2023. Circles display the eddy centers defined from SAR images. The SSHA values are in meters.

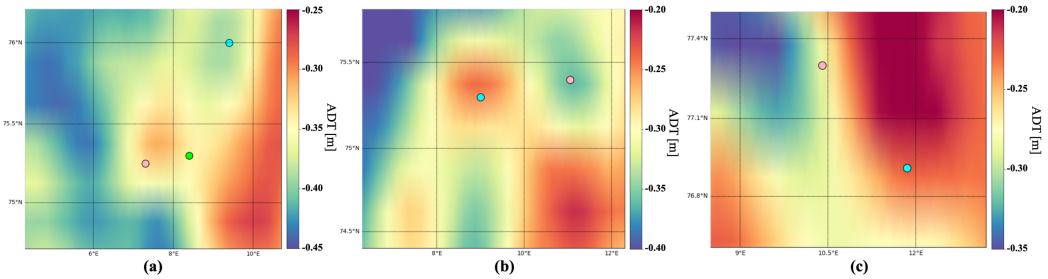

Figure 3. The ADT fields from the L4 product on dates: 28.04 (a), 22.06 (b), 09.07 (c) of 2023. Circles display the approximate eddy centers from the SAR and SWOT data. The ADT values are in meters.

3.2. MIZ Eddies

Figure 4 displays SAR images obtained from Sentinel-1 along with σ_0 values from SWOT satellite passes on the same dates, providing a comprehensive visual comparison of eddies in the MIZ. The first two cases, 02.07 (a–b) and 03.07 (c–d), show similar detected

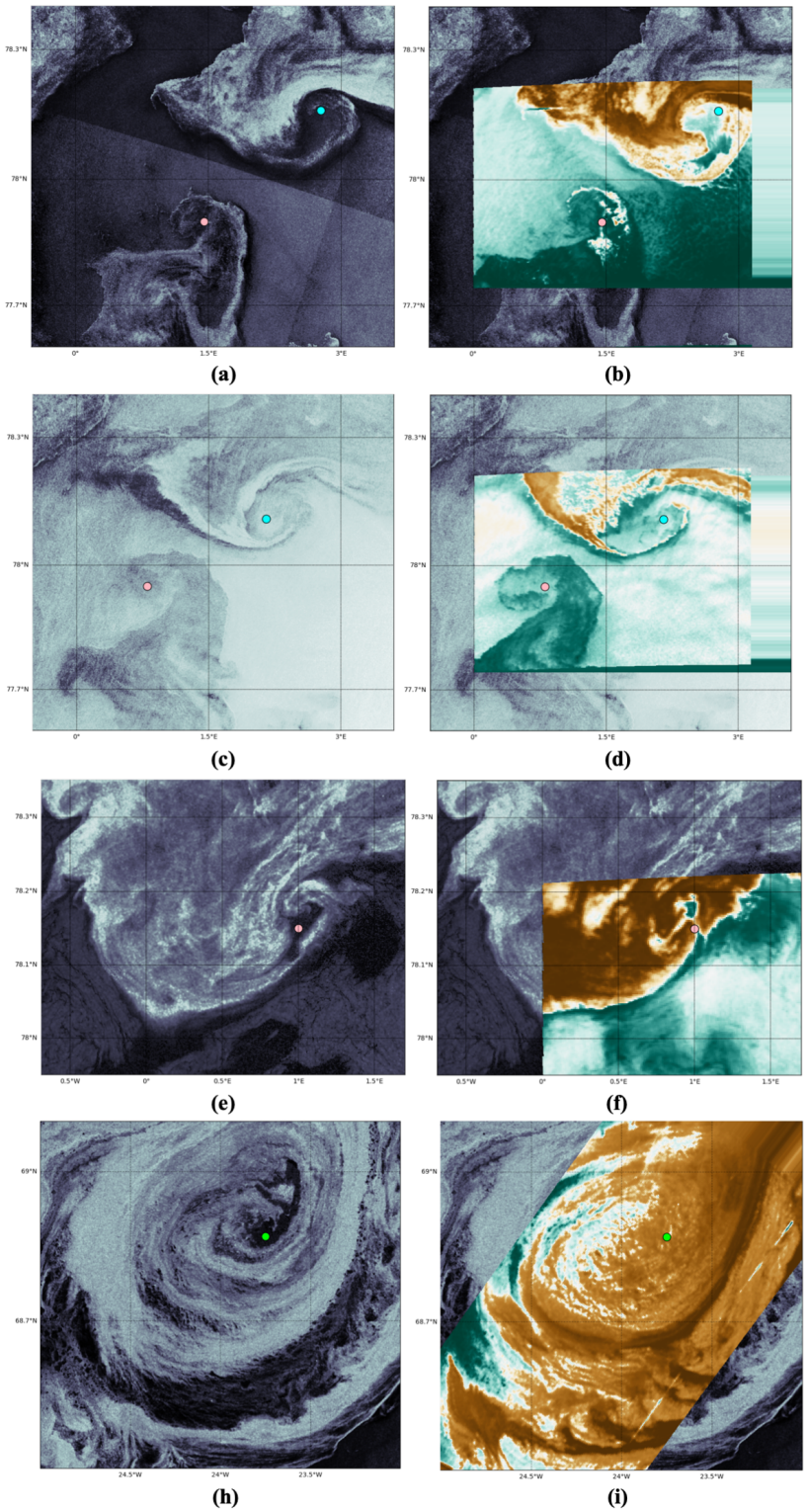

Figure 4. SAR images from Sentinel-1 (left column) and combined SAR and overlaid σ_0 values from SWOT passes (right column) on the same dates: 02.07 (a–b), 03.07 (c–d), 07.07 (e–f), 03.11 (h–i) of 2023. Circles display the approximate eddy centers from SAR images.

eddies under very different sensing conditions, which is especially evident from Sentinel-1. Nevertheless, despite the spatial differences inherent in the resolution and sensing techniques of the two satellites, the structure of the eddies is well-defined in both cases. On 02.07, the eddies are captured under relatively calm sea conditions with lower wind speeds, resulting in moderate backscatter values in the Sentinel-1 images. In the second example, the open ocean appears with very bright pixels in the SAR image, especially in comparison to the previous day. This brightness is primarily due to the stronger and more distinct ocean surface roughness induced by higher wind speeds, enhancing the radar backscatter. Nonetheless, the changes in weather and sensing conditions that may result in backscatter variations do not significantly influence the detectability of the eddies in the MIZ for both Sentinel-1 and SWOT. This consistency underscores the robustness of both sensors in detecting mesoscale and submesoscale ocean features under different environmental conditions.

The third case, representing a single eddy detected on 07.07 (e–f), illustrates a different scenario where the detected eddy is noticeably smaller than the other MIZ eddies used in this study. In this example, the difference in spatial resolution between Sentinel-1 and SWOT becomes more pronounced. Sentinel-1, with its higher spatial resolution, provides more detailed information about the structure of the corresponding eddy, capturing finer details such as the eddy's patterns and edges. SWOT, while offering a smoother image, especially close to the MIZ borders, still successfully identifies the eddy, though with less structural detail. This case highlights the complementary nature of the datasets, where Sentinel-1 excels in high-resolution structural depiction, and SWOT provides broader contextual information.

The fourth case (h–i) depicts a comparison of Sentinel-1 and SWOT for 03.11, illustrating the largest eddy of this study. Here, both sources again provide complementary information regarding the corresponding eddy. Sentinel-1 detailed imagery reveals intricate features of the eddy's structure, such as the vorticity and sub-mesoscale variations within the eddy. SWOT, on the other hand, offers valuable data on the eddy's surface elevation changes and broader spatial context, which are crucial for understanding the eddy's impact on ocean circulation and its role in heat and nutrient transport.

In general, it can be concluded that there is significant agreement between the sensors. The high-resolution structural details captured by Sentinel-1, combined with the extensive swath and elevation data provided by SWOT, enable a comprehensive understanding of eddy dynamics in the MIZ. This synergy between the datasets facilitates improved monitoring and analysis of oceanographic phenomena, ultimately enhancing our ability to study and predict changes in the marine environment.

4. Conclusions

The new altimetry SWOT mission, featuring unprecedented resolution and precision, represents a new era in satellite altimetry and exploration of ocean eddy dynamics. In this study, we present a specific test case on the inter-comparison of the eddy fields in the open ocean and MIZ in the Fram Strait, acquired from SAR and complementary SSHA/σ_0 fields from the new altimetry SWOT mission. The main focus of this study is the analysis and validation of the data from the SWOT mission regarding its capabilities to resolve small eddies in the open ocean area, as well as eddies in the MIZ region. We believe that the presented work can be of interest to the eddy research community, as well as to the CalVal team of the SWOT mission.

Based on a visual examination, we detected and collocated 7 instances of open ocean eddies from both data sources. The most important and obviously expected result is that even at the present CalVal state of the SWOT mission, SSHA fields are clearly capable of resolving small (in our case up to 10 km) submesoscale eddies, which is a huge step forward for satellite oceanography and for the oceanographic community in general. As mentioned earlier, we do not use any kind of interpolation or smoothing for the visualization of SSHA fields in order to avoid distortion and changes in the sizes, locations, and shapes of the eddies. These artifacts are usually caused by interpolation and are typical problems for L4 merged altimetry products.

During data analysis, it became clear to us that the visual interpretation of the open ocean eddy polarity from the SAR images poses a serious problem for the observer. Eddy manifestation in the open ocean is mostly revealed via wave-current interactions, which modulate surface roughness patterns. Such patterns are not always easily interpretable. Even from a very small eddy sample, it is obvious that in certain cases it is impossible to correctly identify the eddy vorticity solely based on the eddy footprint in the SAR image. This is, in our view, a very important result that should be considered by researchers who use SAR data for eddy identification in the open ocean. The visual method for eddy identification from SAR images is widely employed for the exploration of meso-submesoscale eddy variability [*Atadzhanova et al.*, 2017; *Bashmachnikov et al.*, 2020; *Zimin et al.*, 2021]. Additionally, it is used for data labeling to facilitate automatic eddy identification from SAR images through machine learning [*Xia et al.*, 2022; *Zhang et al.*, 2023]. We believe this method can present false results in terms of eddy polarity and should be revised. Given that the revisit time of the SWOT orbit is 21 days, we do not expect that the data from SWOT will completely replace the current approach for eddy identification from SAR in the near future, but rather that both types of data can complement each other, which will greatly improve the accuracy of the final result.

The comparison of the SAR imagery and complementary σ_0 fields for the MIZ region revealed a generally good agreement between both data types. As the coverage of Sentinel-1 and SWOT missions does not always overlap in space and time, these two data sources can complement each other perfectly. Hence, we can conclude that the data from SWOT present a great interest for studying eddies in the MIZ, as well as for other sea-ice applications.

We acknowledge that the sample size presented in our research is limited, and we are not in a position to make far-reaching conclusions. In our future work, we plan to apply the automatic eddy detection methods previously developed and tested on Sentinel-1 SAR imagery [*Khachatrian et al.*, 2023; *Sandalyuk and Khachatrian*, 2025; *Sandalyuk et al.*, 2025] in the MIZ to SWOT data. Combining SWOT and Sentinel-1 observations has the potential to improve eddy detection, particularly for eddies occurring in the open ocean. While the dataset of matched SWOT–Sentinel-1 eddies presented here is a limited test case, similar but more extensive datasets could serve as valuable resources for training or validating machine-learning-based eddy algorithms, such as YOLO, thereby supporting future automated ocean monitoring initiatives.

As was already mentioned above, we understand that further releases will be followed by many upgrades, and we expect that the final product can significantly enhance our understanding of the submesoscale processes in the ocean.

Acknowledgments. This research was funded by the Moscow Institute of Physics and Technology under the State Agreement No. 075-03-2026-305 dated 16.01.2026, with the support of the grant of St. Petersburg University No. 129659573, and The Arctic University of Norway (UiT). The authors would also like to express their gratitude to the SWOT GitHub community for providing comprehensive tutorials on the processing of the SWOT data and to all members of the SWOT project. Sentinel-1 SAR data used in this study are publicly available on the Copernicus Data Space Ecosystem (https://dataspace.copernicus.eu/). The SWOT L2/L3 beta products are publicly available on the AVISO website (https://www.aviso.altimetry.fr). The L4 product from the merged altimetry missions containing ADT fields is publicly available at the Copernicus Marine Environment Monitoring Service portal (https://marine.copernicus.eu/).

References

Appen W.-J. von, Schauer U., Hattermann T., et al. Seasonal Cycle of Mesoscale Instability of the West Spitsbergen Current // Journal of Physical Oceanography. — 2016. — Vol. 46, no. 4. — P. 1231–1254. — https://doi.org/10.1175/jpo-d-15-0184.1.

Atadzhanova O. A., Zimin A. V., Romanenkov D. A., et al. Satellite Radar Observations of Small Eddies in the White, Barents and Kara Seas // Physical Oceanography. — 2017. — No. 2. — https://doi.org/10.22449/1573-160x-2017-2-75-83.

AVISO. SWOT Level-3 Product. Frequently Asked Questions (beta prevalidated, v0.3, Dec 2023). — 2023. — https://www.aviso.altimetry.fr/fileadmin/documents/data/tools/swot_l3_faqL3alphav0_3_rev1.pdf.

Bashmachnikov I. L., Kozlov I. E., Petrenko L. A., et al. Eddies in the North Greenland Sea and Fram Strait From Satellite Altimetry, SAR and High-Resolution Model Data // Journal of Geophysical Research: Oceans. — 2020. — Vol. 125, no. 7. — https://doi.org/10.1029/2019jc015832.

Belonenko T. V., Sandalyuk N. V. and Gnevyshev V. G. Interaction of Rossby waves with the Gulf Stream and Kuroshio using altimetry in a framework of a vortex layer model // Advances in Space Research. — 2023. — Vol. 71, no. 5. — P. 2384–2393. — https://doi.org/10.1016/j.asr.2022.10.042.

Cassianides A., Lique C. and Korosov A. Ocean Eddy Signature on SAR-Derived Sea Ice Drift and Vorticity // Geophysical Research Letters. — 2021. — Vol. 48, no. 6. — https://doi.org/10.1029/2020gl092066.

Chelton D. B., Schlax M. G. and Samelson R. M. Global observations of nonlinear mesoscale eddies // Progress in Oceanography. — 2011. — Vol. 91, no. 2. — P. 167–216. — https://doi.org/10.1016/j.pocean.2011.01.002.

Copernicus. Copernicus Marine Service Quality Information Document. — 2024. — https://catalogue.marine.copernicus.eu/documents/QUID/CMEMS-SL-QUID-008-032-068.pdf.

Dibarboure G., Ubelmann C., Flamant B., et al. Data-Driven Calibration Algorithm and Pre-Launch Performance Simulations for the SWOT Mission // Remote Sensing. — 2022. — Vol. 14, no. 23. — P. 6070. — https://doi.org/10.3390/rs14236070.

ESA. Sentinel-1 Level 1 EW GRD Products. — 2024. — URL: https://dataspace.copernicus.eu/ (visited on 04/18/2024).

Faghmous J. H., Frenger I., Yao Yu., et al. A daily global mesoscale ocean eddy dataset from satellite altimetry // Scientific Data. — 2015. — Vol. 2, no. 1. — https://doi.org/10.1038/sdata.2015.28.

Faugére Ya., Taburet G., Ballarotta M., et al. DUACS DT2021: 28 years of reprocessed sea level altimetry products // EGU General Assembly 2022. — Copernicus GmbH, 2022. — https://doi.org/10.5194/egusphere-egu22-7479.

Fu L.-L., Pavelsky T., Cretaux J.-F., et al. The Surface Water and Ocean Topography Mission: A Breakthrough in Radar Remote Sensing of the Ocean and Land Surface Water // Geophysical Research Letters. — 2024. — Vol. 51, no. 4. — https://doi.org/10.1029/2023gl107652.

Gnevyshev V. G., Malysheva A. A., Belonenko T. V., et al. On Agulhas eddies and Rossby waves travelling by forcing effects // Russian Journal of Earth Sciences. — 2021. — Vol. 21, no. 5. — ES5003. — https://doi.org/10.2205/2021es000773.

Gómez-Navarro L., Cosme E., Sommer J. L., et al. Development of an Image De-Noising Method in Preparation for the Surface Water and Ocean Topography Satellite Mission // Remote Sensing. — 2020. — Vol. 12, no. 4. — P. 734. — https://doi.org/10.3390/rs12040734.

Karimova S. and Gade M. Analysis of sub-mesoscale eddies in the Baltic Sea based on SAR imagery and model wind data // 2015 IEEE International Geoscience and Remote Sensing Symposium (IGARSS). — IEEE, 2015. — P. 1227–1230. — https://doi.org/10.1109/igarss.2015.7325994.

Khachatrian E., Sandalyuk N. and Lozou P. Eddy Detection in the Marginal Ice Zone with Sentinel-1 Data Using YOLOv5 // Remote Sensing. — 2023. — Vol. 15, no. 9. — https://doi.org/10.3390/rs15092244.

Kozlov I. E., Artamonova A. V., Manucharyan G. E., et al. Eddies in the Western Arctic Ocean From Spaceborne SAR Observations Over Open Ocean and Marginal Ice Zones // Journal of Geophysical Research: Oceans. — 2019. — Vol. 124, no. 9. — P. 6601–6616. — https://doi.org/10.1029/2019jc015113.

Kozlov I. E. and Atadzhanova O. A. Eddies in the Marginal Ice Zone of Fram Strait and Svalbard from Spaceborne SAR Observations in Winter // Remote Sensing. — 2021. — Vol. 14, no. 1. — P. 134. — https://doi.org/10.3390/rs14010134.

Kozlov I. E., Plotnikov E. V. and Manucharyan G. E. Brief Communication: Mesoscale and submesoscale dynamics in the marginal ice zone from sequential synthetic aperture radar observations // The Cryosphere. — 2020. — Vol. 14, no. 9. — P. 2941–2947. — https://doi.org/10.5194/tc-14-2941-2020.

Malysheva A., Belonenko T. and Koldunov A. Agulhas leakage estimation using altimetry and Argo data // Issledovanie Zemli iz Kosmosa. — 2020. — No. 2. — P. 24–34. — https://doi.org/10.31857/s0205961420020049. — (In Russian).

Morrow R., Fu L.-L., Ardhuin F., et al. Global Observations of Fine-Scale Ocean Surface Topography With the Surface Water and Ocean Topography (SWOT) Mission // Frontiers in Marine Science. — 2019. — Vol. 6. — https://doi.org/10.3389/fmars.2019.00232.

Nurser A. J. G. and Bacon S. Eddy length scales and the Rossby radius in the Arctic Ocean // Ocean Science Discussions. — 2013. — Oct. — Vol. 10. — P. 1807–1831. — https://doi.org/10.5194/osd-10-1807-2013.

Pujol M.-I., Faugére Ya., Taburet G., et al. DUACS DT2014: the new multi-mission altimeter data set reprocessed over 20 years // Ocean Science. — 2016. — Vol. 12, no. 5. — P. 1067–1090. — https://doi.org/10.5194/os-12-1067-2016.

Sandalyuk N., Belonenko T. and Koldunov A. Shelf Waves in the Great Australian Bight Based on Altimetry Data // Issledovanie Zemli iz Kosmosa. — 2020a. — No. 6. — P. 73–84. — https://doi.org/10.31857/s0205961420050085. — (In Russian).

Sandalyuk N. and Khachatrian E. Automatic eddy detection in the MIZ based on YOLO algorithm and SAR images // Science of Remote Sensing. — 2025. — Vol. 11. — P. 100228. — https://doi.org/10.1016/j.srs.2025.100228.

Sandalyuk N., Khachatrian E. and Marchuk E. Automatic eddy detection in Antarctic marginal ice zone using Sentinel-1 SAR data // Frontiers in Marine Science. — 2025. — Vol. 12. — https://doi.org/10.3389/fmars.2025.1648021.

Sandalyuk N. V. and Belonenko T. V. Mesoscale vortex dynamics in the Agulhas Current from satellite altimetry data // Sovremennye problemy distantsionnogo zondirovaniya Zemli iz kosmosa. — 2018. — Vol. 15, no. 5. — P. 179–190. — https://doi.org/10.21046/2070-7401-2018-15-5-179-190. — (In Russian).

Sandalyuk N. V., Bosse A. and Belonenko T. V. The 3-D Structure of Mesoscale Eddies in the Lofoten Basin of the Norwegian Sea: A Composite Analysis From Altimetry and In Situ Data // Journal of Geophysical Research: Oceans. — 2020b. — Vol. 125, no. 10. — https://doi.org/10.1029/2020jc016331.

SWOT. SWOT Level 2 KaRIn Low Rate Sea Surface Height Data Product Version 1.1. — 2023. — https://doi.org/10.5067/SWOT-SSH-1.1.

Travkin V. S. and Belonenko T. V. Seasonal variability of mesoscale eddies of the Lofoten Basin using satellite and model data // Russian Journal of Earth Sciences. — 2019. — Vol. 19, no. 5. — ES5004. — https://doi.org/10.2205/2019es000676.

Tréboutte A., Carli E., Ballarotta M., et al. KaRIn Noise Reduction Using a Convolutional Neural Network for the SWOT Ocean Products // Remote Sensing. — 2023. — Vol. 15, no. 8. — P. 2183. — https://doi.org/10.3390/rs15082183.

Wekerle C., Hattermann T., Wang Q., et al. Properties and dynamics of mesoscale eddies in Fram Strait from a comparison between two high-resolution ocean-sea ice models // Ocean Science. — 2020. — Vol. 16, no. 5. — P. 1225–1246. — https://doi.org/10.5194/os-16-1225-2020.

Xia L., Chen G., Chen X., et al. Submesoscale oceanic eddy detection in SAR images using context and edge association network // Frontiers in Marine Science. — 2022. — Vol. 9. — https://doi.org/10.3389/fmars.2022.1023624.

Zhang D., Gade M., Wang W., et al. EddyDet: A Deep Framework for Oceanic Eddy Detection in Synthetic Aperture Radar Images // Remote Sensing. — 2023. — Vol. 15, no. 19. — P. 4752. — https://doi.org/10.3390/rs15194752.

Zimin A. V., Atazhanova O. A., Romanenkov D. A., et al. Submesoscale Eddies in the White Sea Based on Satellite Radar Measurements // Izvestiya, Atmospheric and Oceanic Physics. — 2021. — Vol. 57, no. 12. — P. 1705–1711. — https://doi.org/10.1134/s0001433821120306.